ACTA IMEKO
ISSN: 2221-870X
February 2015, Volume 4, Number 1, 5 - 10

Preliminary study of an ancient earthquake-proof construction technique monitoring by an innovative structural health monitoring system.

Carmelo Scuro[1], Domenico L. Carnì[2], Francesco Lamonaca[3], Renato S. Olivito[4], Gabriele Milani[5]

[1] *Department of Physics, University of Calabria, 87036 Rende (CS), Italy*
[2] *DIMES - Department of Informatics Modelling Electronics and Systems Science, University of Calabria, 87036 Rende (CS), Italy*
[3] *DING - Department of Engineering, University of Sannio, 82100 Benevento, Italy*
[4] *DINCI – Department of Civil Engeneering, University of Calabria, 87036 Rende (CS), Italy*
[5]*Department of Architecture, Built Environment and Construction Engineering, Technical University of Milan, 20133 Milan, Italy*

ABSTRACT
When analyzing the historical and cultural heritage at world level, what is present in the Italian territory becomes of great importance, because this territory is one of the richest in the world. Often, not always, one is aware of everything that is present in this territory, and with new studies, more and more extraordinary discoveries are made in the field of historical buildings. In particular, a new discovery was made in Calabria in the field of structural engineering. By analyzing various architectural treatises related to earthquake-proof constructions, a patent for an earthquake-resistant construction, made with fictile tubules bricks, was found.
In this work, the researchers, after conducting several experimental studies, propose an innovative method to monitor and obtain the mechanical properties of these structures in real time, minimizing measurement uncertainty.

Section: RESEARCH PAPER

Keywords: Anti-seismic Technique; Experimental Test; Numerical Analysis; Structural Health Monitoring Systems; Measurement Accuracy.

Citation: Thomas Bruns, Dirk Röske, Paul P.L. Regtien, Francisco Alegria, Template for an IMEKO event paper, Acta IMEKO, vol. 3, no. 1, article 1, January 2014, identifier: IMEKO-ACTA-03 (2014)-01-01

Editor: Paolo Carbone, University of Perugia, Italy

Receivedmonthday, year; **In final form**month day, year; **Published**January2014

Funding: This work was supported by Measurement Science Consultancy, The Netherlands

Corresponding author: Carmelo Scuro, e-mail: carmelo.scuro@unical.it

1. INTRODUCTION

In the safeguarding and prevention of possible collapses of structures of historical interest, the collection of information relating to the quality of construction materials, environmental actions, the propensity for an alteration of a single component or of the structure in its entirety caused by loss of strength in the time of materials and by accidental events, becomes of fundamental importance [1-2].

Structural Health Monitoring systems (SHM), as previously mentioned, guarantee, for different types of engineering structures, and in particular for historic buildings, to characterize, identify and detect the evolution of damage and degradation in these [3]. In the field of structural monitoring, the SHMs systems are made up of two main parts; an acquisition system that allows the transmission and recording of information, and the sensors connected to it, also via wi-fi, which evaluate the different physical quantities [4]. In particular, the main information provided by the SHM systems are: temperature, displacement, strain, acceleration, tensile stress and compressive strength and so on [5]. Almost all SHM systems are placed in structures in a non-invasive way and through a reversible process using sensors that are placed in very precise control points of the structure. It is made in order to optimize the use of fewer sensors to minimize unnecessary costs and information [6]. The useful information acquired by the sensors, after having undergone a check, are used in mathematical numerical models of the structures in order to determine the evolution of possible damage and safety [7]. In recent years, structural monitoring systems have been improved by applying the Internet of Thighs (IoT) paradigm. This is due to the fact that in the IoT paradigm, each node is capable of processing, detecting and transmitting data. The information, through an internet connection, is transmitted and stored in a Cloud, and processed by distributed systems made functional by a Big Data paradigm [8]

The ultimate purpose of this paper is to carry out a preliminary study related to the use of an SHM system to be placed on an ancient anti-seismic structure made using a patent from the beginning of 1900.

Figure 1. Example of *opus craticium i*n Herculaneum, Italy [10]

The first anti-seismic masonry constructions in history were characterized by the use of timber frames and is part of the cultural heritage of several countries. Timber frame buildings are denoted by different names and are characterized by various geometries in each country [9-10]. Their popularity is due to their easy assembly and low cost, especially in areas with abundant availability of wood (e.g., North America, Portugal, Scandinavia, United Kingdom) and to their satisfying structural performance in seismic-prone areas (e.g. Central and South America and Mediterranean countries).

In the latter case, timber frames are usually employed in shear walls where they are combined with light-weight masonry [11]. Many buildings built with this technology have endured to this day. This is due to the fact that by using this construction method, buildings are able to increase their resistance to strong dynamic stresses.

The "*Edificios pombalinos*", in Portugal, is one of the first great European examples of a building characterized by a wooden frame structure [12-13]. In the aftermath of the Great Lisbon earthquake of 1755, the city was rebuilt employing a construction technology with outer masonry walls enclosing an inner three-dimensional timber frame. This consisted of horizontal and vertical elements, held together by diagonal bracing members [14].

In Italy, archaeological excavations in Herculaneum revealed a two-story building erected with a half-timber technology matching the one that Vitruvius called *opus craticium* and dealt with in his masterpiece De architectura [10] (Figure 1). A different and relatively unknown technique, called "*casa baraccata*", originated during the 17th century in the Southern region of Calabria.

Calabria, a region of southern Italy, is one of the zones most exposed to seismic risk in the Mediterranean area. After the catastrophic seismic events that hit the region in 1638, many structures were rebuilt with the "*casa barracata*" system. This technology is similar to the *edificios pombalinos* mentioned above, and uses a wooden frame (called *Beneventana*) made with vertical columns spaced from each other by 1.2 meters and connected with horizontal beams and diagonal elements, as shown in Figure 2 [15]. This robust frame provides the building with both sufficient stiffness and ductility to withstand huge dynamic loads. Relevant examples of such technology is the bishop's house in Mileto (about 10 km Southwest of Vibo Valentia) which is described to have undergone practically no damage during the 1783 earthquake [16].

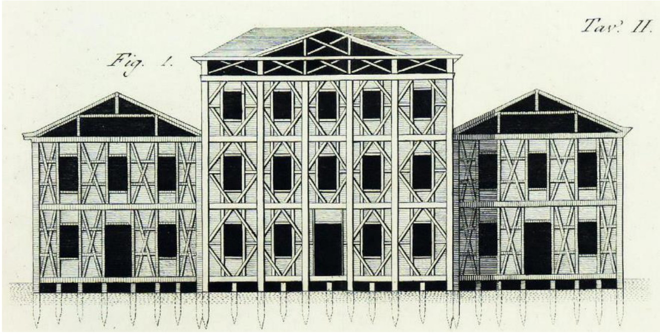

Figure 2. Visual conception of casa *baraccata* [17]

On December 28, 1908, the deadliest earthquake ever occurred in Italy destroyed the cities of Messina, Sicily, and Reggio Calabria. This earthquake was characterized by an estimated moment of magnitude 7.1 and caused over 100,000 victims. The two main cities were totally destroyed, while the structures of the nearby towns collapsed partially, except those built with a particular cylindrical hollow clay brick identified with the name of fictile tubules [18]. These particular construction elements, identified as the first hollow bricks of the history, are characterized by a medium-high compressive strength when compared with other hollow bricks. The overall reduction in the weight of the structure is due to their hollow shape, which also guarantees the decrease in the building's participating mass during a seismic event, limiting the formation of cracks and improving the stability of the constructions [19]. During the main phases of the reconstruction of the city of Reggio Calabria and Messina in 1909, a Calabrian engineer, Pasquale Frezza, patented a construction technique for an anti-seismic structure invented by evolving the concept of the *casa baraccata*. The main purpose of this patent was the inclusion of fictile tubules in the construction of the filling walls of the wooden frames. This was made to guarantee lightness to the structure, and ease of construction, because the potters, widespread in the area, could quickly make these hollow bricks. Specifically, the new technique consisted of masonry walls built inside the wooden structure, alternating common bricks and fictile tubules, thus removing the diagonal wooden reinforcement elements, as shown in Figure 3 [20].

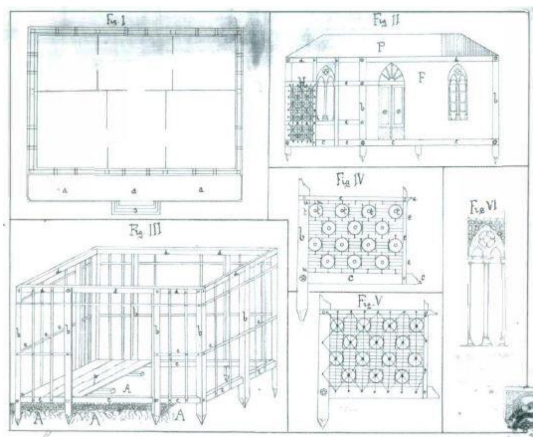

Fig. 3. Pasquale Frezza's patented design [21]

The paper is organized as following. Preliminary, the theory of structural mechanics used in order to calculated the shear strength in the specimens was exposed. Successively, experimental test is introduced and the results explained. In the section three, the numerical model obtained by software at finite element ABAQUS is proposed. Following, the experimental testbed was described and the measurement accuracy is determined, and the conclusions are drawn.

2. LICTERATURE CRITERIA FOR THE SHEAR STRENGTH PREDICTION OF PIERS

Several simplified models are listed in the literature and in various codes for the descriptions of the type of damage that may occur in masonry piers. These models are based on the evaluation (not accurately) of the local/mean stress generated by forces applied on pre-identified points/sections of the pier [22]. The most frequent failure modes that occur in piers are rocking/crushing, bed joint sliding and diagonal cracking; the type of damage that was most highlighted during the experimental tests conducted in laboratory, and exposed in the third paragraph, is the last listed.

For the Diagonal Cracking failure mode two models are usually adopted to describe it [23,24]. These models are used to describe different types of masonry and often provide different strength values. In the Mann and Müller model the limit strength domain is defined by means of "local" type parameters relating to the individual materials that composed the masonry (mortar and bricks) such as the cohesion and friction coefficient in the mortar joints and the tensile strength of the block of masonry under analysis [23]. These two types of parameters are, generally, obtained experimentally, and the individuation of the cohesion and friction coefficient can be difficult for particular masonry such as that in fictile tubules.

In the Turnšek and Čačovič model, the domain is defined through a single parameter of the material: the tensile strength of the masonry, usually determined by the diagonal compression test [24].

In order to study Diagonal Cracking, it is possible to recognize two main types of models: (I) the model proposed by Mann and Müller, that describe the masonry as a composite material and considers the develop of the cracks, separately, along bricks and mortar joints; (II) the model proposed by Turnšek and Čačovič, that considered the masonry as an equivalent isotropic material and describing indistinctly the development of damage along principal stress directions [25].

The application of the Mann and Müller formulation to a masonry wall made with bricks and fictile tubules becomes difficult. It is based on two main hypotheses: (I) the mechanical properties of head joints are negligible, and in the case in question the bricks have a square section; (II) bricks are much stiffer than mortar joints, but the tubules are hollow and have a cylindrical conformation, and this hypothesis cannot be satisfied.

In light of this, it was decided to use the formulation of Turnšek and Čačovič that considers the masonry as an isotropic material. The reference stress σ_c, the maximum principal stress acting at the centre of the pier σ_I must not exceed the tensile strength of masonry f_t. This last parameter is assumed as constant in any loading direction (isotropic limit stress domain) [26]. This was possible because the authors, in previous works, carried out a homogenization of the material with which the wall was made [18;27].

The Maximum principal stress at the center of the pier was calculated with the following equation:

$$\sigma_I = \frac{\overline{\sigma_y}}{2} + \sqrt{\left(k_{1d}\,\bar{\tau}\right)^2 + \left(\frac{\overline{\sigma_y}}{2}\right)^2} \tag{1}$$

where: $\bar{\tau}$ and $\overline{\sigma_y}$ are the mean shear and normal stresses acting on the cross section of the pier and k_{1d} is the ratio between the shear stress at the center of the pier and the mean shear stress [24]. The Failure criteria for masonry piers, represented in the resolved stress plane is shown in Figure 4.

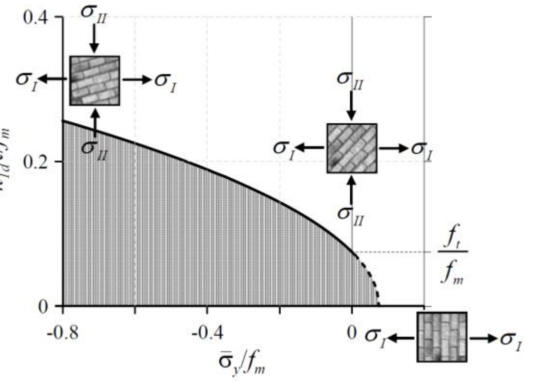

Fig. 4. The Failure criteria of Turnšek and Čačovič for masonry piers, represented in the resolved stress plane [25]

In the new Italian technical standards (document C8.7.1.3.1.1 7/2019) there is a simplification of the formulation of Turnšek and Čačovič in order to obtain the value of shear strength of the masonry pier. Figure 5 shown the schematization adopted of the masonry block.

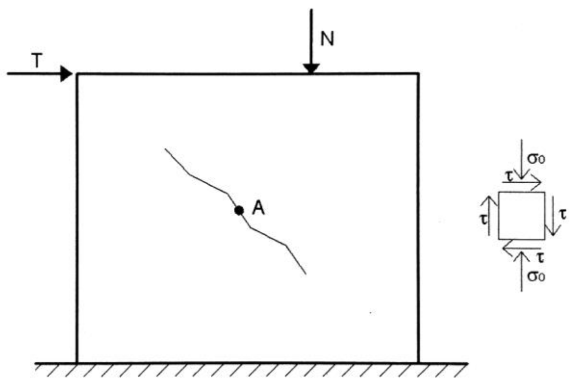

Fig. 5. Schematization adopted of the masonry block.

The normal and tangential stress was calculated in the point A whit the following equations:

$$\sigma_0 = \frac{N}{l \cdot t} \tag{2}$$

$$\tau_0 = \frac{T}{l \cdot t} \tag{3}$$

Where T and N are respectably the shear and normal force applied to the masonry block, and l and k are the length and thickness of the masonry. The stress state at point A is represented by Mohr's circle in Figure 6 characterized by center C and radius R, expressed by equation 4 and 5:

$$C = \frac{\sigma_0}{2} \tag{4}$$

$$R = \sqrt{\left(\frac{\sigma_0}{2}\right)^2 + \tau^2} \tag{5}$$

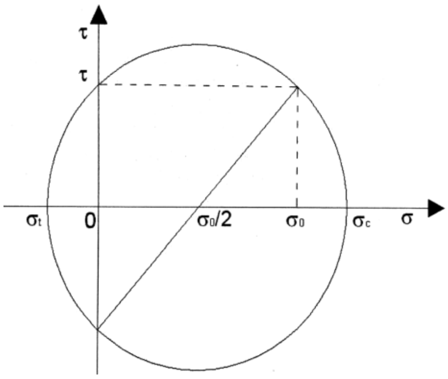

Fig. 6. Tensile state in the point A.

The principal tensile stress that occurred in the masonry it is obtained by the following equation:

$$\sigma_t = C - R = \frac{\sigma_0}{2} - \sqrt{\left(\frac{\sigma_0}{2}\right)^2 + \tau^2} \tag{6}$$

squaring equation 6 and simplifying we obtain:

$$\tau^2 = \sigma_t^{\,2} - \sigma_t \cdot \sigma_0 \tag{7}$$

if - σ_t (tensile stress in the masonry) is equal to f_t, tensile strength of masonry imposed like a limit domain of Turnšek and Čačovič, and $\tau = b \cdot \tau_0$, the equation number 7 becomes:

$$\tau_0 = \frac{f_t}{b}\sqrt{1 + \frac{\sigma_0}{t}} \tag{8}$$

multiplying by the area of the section the shear strength of the masonry pier is obtained:

$$V_s = \frac{f_t \cdot l \cdot t}{b}\sqrt{1 + \frac{\sigma_0}{t}} = \frac{1.5 \cdot l \cdot t \cdot \tau_{0d}}{b}\sqrt{1 + \frac{\sigma_0}{1.5 \cdot \tau_{0d}}} \tag{8}$$

Where:

- V_s is the shear strength of the masonry pier obtained for overcoming of limit domain.
- f_t is the tensile strength of masonry.
- b is a coefficient that takes into account the slenderness of the element. It is the ratio between height and length of the pier, its value is in the range between 1 and 1.5.
- τ_{0d} is the reference shear strength

3. EXPERIMENTAL CAMPAIGN

The experimental campaign was conducted in the laboratories of the University of Calabria and was divided into two well-defined steps. Using the same construction process, two masonry walls were made following the patent of the engineer Pasquale Frezza [28]. The first was tested by diagonal compression test and stopped after the specimen collapsed. The second specimen was tested in the same way, but was first damaged and then repaired with Basalt Fiber Reinforced Cementitious Matrix (B-FRCM). After that, the test was repeats until collapsed of the reinforced masonry wall.

3.1. Preparation of the specimens

The dimensions of the two specimen walls are 60×60×15 cm^3. The external timber frame is constructed in a carpentry workshop and consists of four poplar beams with a cross-section of 15×5 cm^2 (poplar is a typical wooden building materials used for the constructions in Calabria). The connection between contiguous beams is ensured by cutting their extremities to make half-lap fastenings and then bolting them together with four iron screws.

After the outer timber frame is built, the inner masonry wall is realized. The bricks used have a square cross-section of 5.5 cm per side and a height of 13 cm. The fictile tubules are nomenclating NFTs (New Fictile Tubules) [18;27] since they are produced in a potter industry with faster and innovative techniques, and then refined on the potter's wheel. They are characterized by the same height of the bricks (13 cm) and present a thickness of 6 mm (Figure 7, Figure 8). The mortar is characterized by a compressive strength of about 2.5 MPa and corresponds to the one labelled as M2.5 *bastarda* according to Table 11.10.IV of the 2008 Italian Building Code. This particular mortar consists of 1 part of cement, 2 of lime mortar and 9 of sand.

The specimen wall is completed by casting a 2 cm thick layer of mortar to cover the tips of the fictile tubules (Figure 9).

Fig. 7. Arrangement of bricks and NFTs in the timber frame.

Fig. 8. Mortar casting.

Fig. 9. Creation of the upper layer of mortar.

3.2. Diagonal compressive test on the first specimen

The diagonal compressive test is carried out by rotating the specimen wall of 45°; two steel caps are placed on the specimen, one at the bottom for support and the other at the top for uniformly distributing the load. The speed of the test is 0.5 mm/s. Two couples of transducers are applied to the masonry specimen to further monitor the relative displacements: those referred to as LVDT0 measure vertical displacements between two bricks, whereas those referred to as LVDT1 measure horizontal displacements between two fictile tubules (Figure 10).

Another transducer that has the same characteristics, as those used for calculating the displacements of the masonry, was positioned near the upper part of the load cell in order to measure the lowering of the cross member of the test machine.

The load-displacement diagram is shown in Figure 11: after a linear elastic branch up to 80% of the maximum load, the diagram displays a decrease in the elastic modulus and reaches a plateau, where the peak load is attained and is equal to 51.48 kN. at this load value, the displacement of the load cell, recorded by the third transducer, is equal to 11.526 mm. The hardening branch is most likely due to friction between mortar and the fictile tubules elements, and to the overall compressive stress state of the specimen wall.

Fig. 10. Set up of the test.

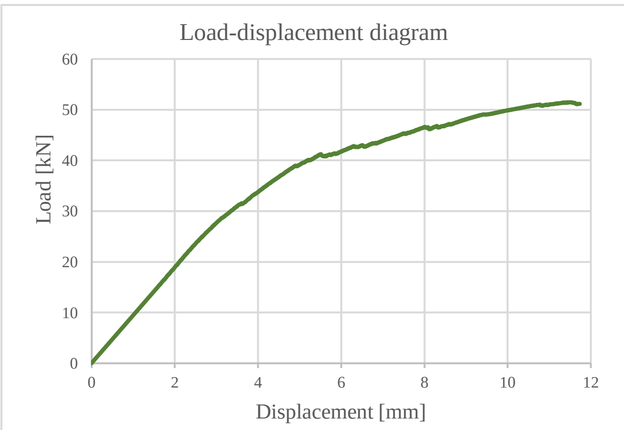

Fig. 11. Load-displacement diagram

The shear strength of the wall S_s is evaluated using equation (9) as suggested by [29]:

$$S_S = \frac{0.707 \cdot P}{A_n} \qquad (9)$$

P is the peak load and A_n is the net area which is evaluated according to equation (10):

$$A_n = \left(\frac{w+h}{2}\right) t \cdot n \qquad (10)$$

w and h are respectively the width and the height of the specimen (here considered as the dimensions of the masonry inner core and both equal to 50 cm), t is the thickness of the specimen (15 cm) and n is a coefficient related to the rate of voids in the specimen (here considered equal to 0.6 where 1 corresponds to a wall with no voids). The shear strength corresponding to the peak load is 0.81 MPa.

Figure 12 shown the Load Vs Displacement diagrams recording by transducers during the test.

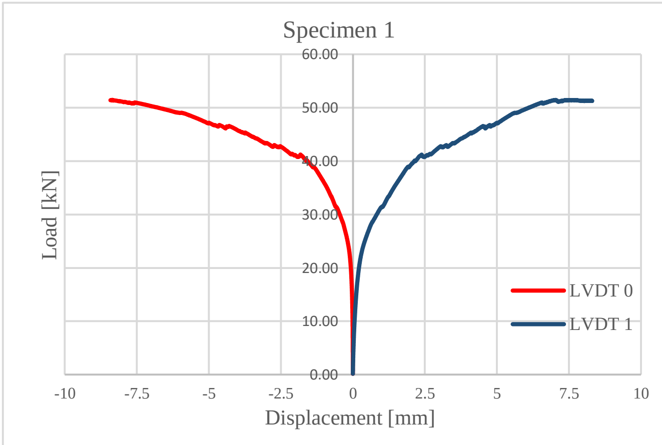

Fig. 12. Load vs Displacement diagrams of transducers for specimen 1

3.3. Diagonal compressive test on the second specimen

The same test set up was used to perform the analyses on specimen number 2. In this case, the test was stopped at the formation of the first damage and when the diagram was arrived to the finish of a linear elastic branch. The recorded peak load is equal to 46 kN (Figure13).

The shear strength of the wall Ss was evaluated using equation (9); the value corresponding to the peak loads is equal to 0.73 MPa.

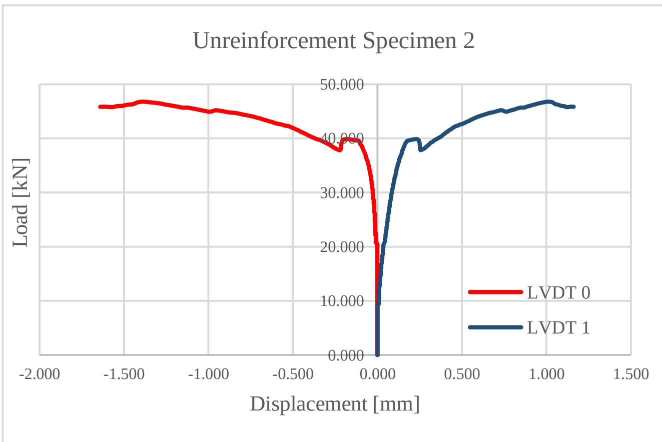

Fig. 13. Load vs Displacement diagrams of transducers for unreinforcement specimen 2

When the first damage developed in the specimen, the test was stopped, and the specimen was repaired and reinforced.

Three Basalt-FRCM strips of 100 mm were placed at the side of the wall characterized by the layer of two cm of mortar (Figure 14). The B-FRCM is chosen because guarantees compatibility with the support and is characterizes by: tensile strength and Young's modulus for basalt fibers equal to 301.5 MPa and 16 GPa respectively, while those for B-FRCM are 134 MPa and 19 GPa [11]. In order to measure the strains on them, two strain gauges were applied at central strip in correspondence of the fibers perpendicular to the cracks. Then, the test was repeated on the reinforced specimen until collapse.

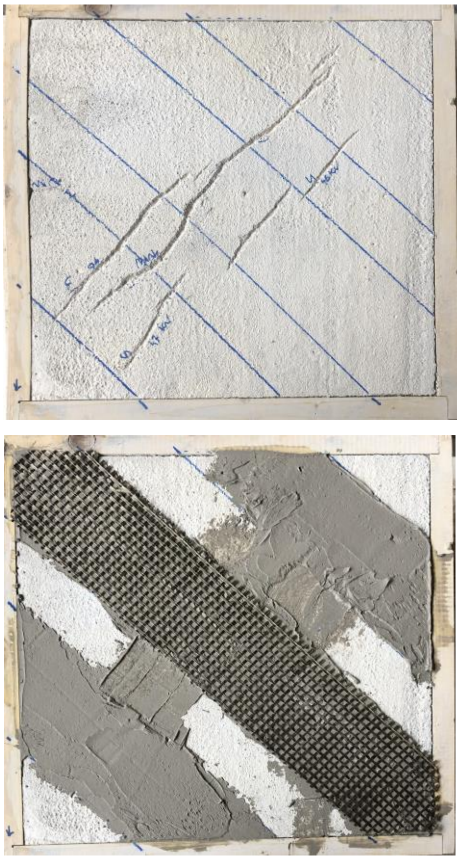

Fig. 14. Specimen 2 before and after reinforcement

The maximum value of the load recorded during the reinforced test is equal to 66.48 kN (Figure 15). At this load value, a failure of the Basalt-FRCM (B-FRCM) reinforcement occurred [30-31]. The collapse of the reinforcement strip happens through debonding with cohesive failure of the substrate (Figure 16).

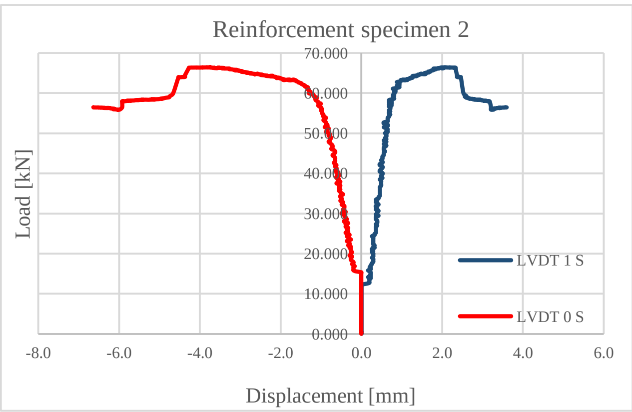

Fig. 15. Load Vs Displacement diagrams of transducers for reinforcemt specimen 2

In order to obtain the value of the strain that occurred in the reinforced basalt fiber during the test, two strain gauges ware applied in central part of the diagonal BFRP.

A strain gauge is a device commonly used in order to obtain the strain on a specimen subject to different type of stress, for example compression or tensile stress.

Fig. 16. Collapse of the reinforcement strip

The strain gauges employed in the test are the most common type and consists of an insulating flexible backing which supports a metallic foil pattern. The gauge is positioned on the strip of B-FRCM with a cyanoacrylate. When the basalt fibers are deformed, the foil is deformed, causing its electrical resistance to change. This resistance change, usually measured using a Wheatstone bridge, is related to the strain by the quantity known as the Gauge factor.

Figure 17 shown the diagram Shear Stress Vs Strain obtained during the test conducted on the reinforced specimen.

The Shear Stress was evaluated by the equation number 9 and in this case is equal to 1.04 MPa.

The average value of the strain recorded during the test by the two strain gauges was 3.25 [µm/m] E-3. This value is in accordance with the value prescribed by the manufacturer of the fiber that certifies it among the 3- 3.5 [µm/m] E-3.

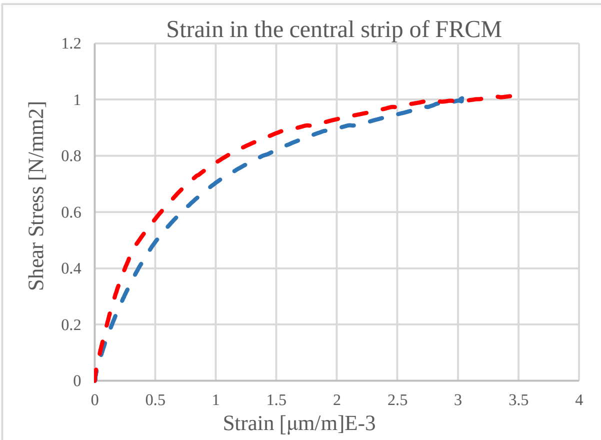

Fig. 17. Shear Stress Vs Strain

4. NUMERICAL MODEL

The principal goal of the creation of numerical model is those to repeat the diagonal compressive test and to simulate the behaviour of these structures. The commercial CAD software Rhinoceros was employed in order to create a simplified geometrical model of the specimen. The outer timber frame, the common bricks, the fictile tubules are apart modelled like a solid composed by surface characterized by normal vector facing out [33]. After that, the single part is assembled and imported together into the commercial FE software Abaqus, where the analysis is conducted.

The common brick and the timber frame are meshed using hexahedral C3D8 finite elements (classified C3D8 in Abaqus), while tetrahedral elements (C3D4) are used for the fictile tubules and inner mortar. The final model created is composed to a total of 47093 nodes and 165710 elements (1120 C3D8 and 164590 C3D4) [15;18]. In order to the behaviour of their bond, a tie constraint is imposed between mortar and fictile tubules and bricks. a general contact is imposed to simulate the interaction between timber frame and mortar, imposing a friction coefficient of 0.8 [34].

The material of common bricks and timber frame is modelled like linear elastic material, in the specific, the orthotropy of the wood is not consider, but this is imposed as a isotropic material in order to simplify the final model and reduce the computational burden [35]. It is possible because, during the experimental test, the timber frame is damaged after the mortar and it is not arrived to collapse. Instead, fictile tubules and mortar are simulated using CDP material model (Concrete Damaged Plasticity), available in the Abaqus library. Originally, the CDP was created to simulated the behaviour of concrete under fairly low confining pressure, taking into account the damage that develops in it, its general formulation allows its use in the simulation of a broader range of materials [36-38]. Table 1 lists the Young's moduli and Poisson's ratios for the four materials here considered. Table 2 and Table 3 display the tensile constitutive law for fictile tubules and mortar, respectively, expressed in terms of displacements and stresses.

Table 1 Values of Young's modulus and Poisson's ratio.

Material	Young's modulus [MPa]	Poisson's ratio [-]
Wood	270	0
Clay (bricks)	1290	0.15
Clay (tubules)	4800	0.15
Mortar	275	0.2

Table 2 Tensile constitutive law for mortar.

Tensile stress [MPa]	Plastic displacement [mm]
0.42	0
0.0005	0.03
0.0005	6.5

Table 3 Tensile constitutive law for tubules' clay.

Tensile stress [MPa]	Plastic displacement [mm]
2.75	0
0.0005	0.058
0.0005	10.75

Figure 18. Comparison of cracks development in in the back and front side of numerical model and experimental specimen wall.

The ultimate displacement of the materials is imposed with high value in order to complete successfully the analysis without affecting the structural response of the materials. A damage parameter of 0.99 is set for both mortar and the tubules' clay in proximity of a plastic displacement equal to 0.03 mm.

The comparison between the numerical and experimental load-displacement diagrams is shown in Figure 19. The numerical analysis satisfactorily estimates the linear elastic branch of the graph, but the peak load attained is 8% higher than the experimental one (55.54 kN against 51.48 kN). Also, the numerical analysis halts for an ultimate displacement which is close to that related to the load peak recorded during the experimental test. In fact, the displacement obtained by the numerical model is 11.700mm, the experimental one 11.526 mm.

The damage in numerical model corresponds to the experimental outcome, while displaying more cracks at the top and four single cracks departing from the midsection of each timber beam. Given the overall fair correspondence in terms of crack patterns, it can be assumed that these four single cracks appear only for numerical reasons, therefore they play no effective role in the overall response of the numerical model (Figure 18).

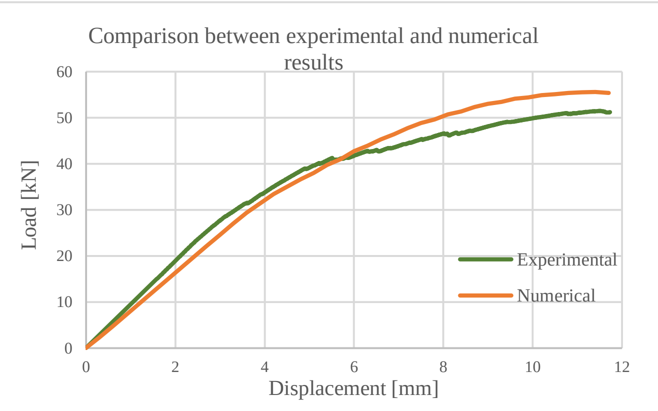

Fig. 19. Shear Stress Vs Strain

5. EXPERIMENTAL TESTBED AND MEASUREMENT ACCURACY

Two different Acquisition System (AS) was used in order to monitoring the displacements, in the case of first specimen, and the displacement and the strain of the basalt fibber in the case of second specimen.

The first AS was composed as following: three Linear Variable Differential Transformer (LVDT) [39], used for monitoring the horizontal and vertical displacement, were connected to data acquisition system (DAQ) Spider-8 which transmitted the data to a computer. The second was composed of two LVDT and two strain gauges, which were connected at DAQ 5100B of System Micromeasurement. The second DAQ permits to acquire, in real time, two different types of data that were transmitted to a computer in order to processing them in real time.

The LVDTs used to monitoring the displacement in the masonry wall are the type WA-T 50 mm and are procured by HBM and are. The displacement transducers WA-T are in probe version and they use an active quarter bridge circuit based on the differential inductor principle. The bridge is also directly integrated in the sensor to create a full bridge circuit for easy connection of the WA-T transducer to DAQ. The linearity variation in relation to nominal value is ±1% range of displacement that it is possible to measure with this type of LVDTs is 0-50 mm. The electronic scheme of the LVDT WA-T is shown in Figure 20.

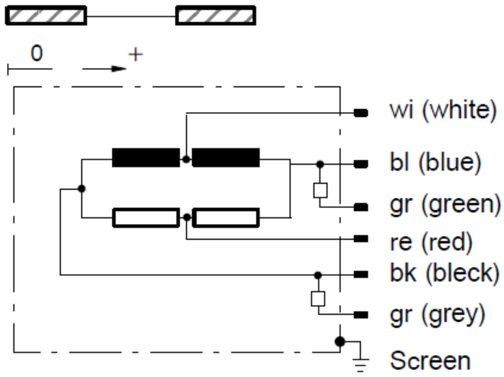

Fig. 20. Electronic scheme of LVDT WA-T [40]

The DAQ, Spider 8, was used by an individual operator and has ensured: Simultaneous measurement acquisition, high sampling rate at 16-bit resolution and selectable digital filters. The linearity variation in relation to nominal value is ±0.05 %.

System 5000's Model 5100B Scanners acquire test data within 1 millisecond from up to 1200 channels at scan intervals as short as 0.02 s. This permits to have more accurate test results, and the ability to capture data under static loading conditions immediately before failure of the structure monitored. The Strain gauge cards integrated, include built-in bridge completion for quarter and half bridges, and a constant voltage power supply for 0.0, 0.5, 1.0, 2.0, 5.0, and 10.0 VDC bridge excitation. The A/D CONVERTER is characterized by 16-bit successive approximation converter with 40 µs total conversion time per reading.

The 5100B operate with 1 ms per scan. Fifty complete scans per second typical usage. Concurrent scanning for all scanners. Input channels in each single scanner are scanned sequentially at 0.04 ms intervals and stored in random access memory within a 1 ms window.

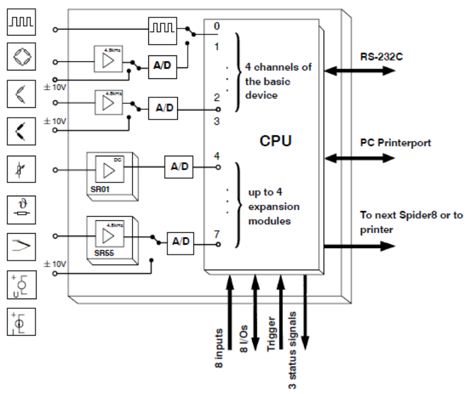

Fig. 21. Electronic scheme of LVDT WA-T [41]

The strain gauges employed are of the type PFL-10-1. They are Polyester linear gauges with mild steel compensation. This is a foil strain gauge having polyester resin backing. This type of strain gauges is characterized by 2 cm lead wires pre-attached, Strain Limit of 2 % (20000 µstrain), operational temperature [20, 80] °C and nominal resistance equal to 120 Ω.

The main problem detected during the second test on the second specimen was the return of the LVDT data.

As shown in figure 15 in the elastic branch of the Load Vs Displacement diagram there is a disturbance caused by a noise due to the DAQ. The data acquired instead by the channels dedicated to the strain gages do not present this problem. For this reason, a spline fitness function has been implemented to minimize the effect of the noise preserving the linearity of the Load Vs Displacement graphs, obtaining new diagrams shown in Figure 22. In particular, on the data acquired a cubic spline interpolation algorithm is used. The spline function smooths the random trend due to the noise, permitting to highlight the trend of the load vs the displacement.

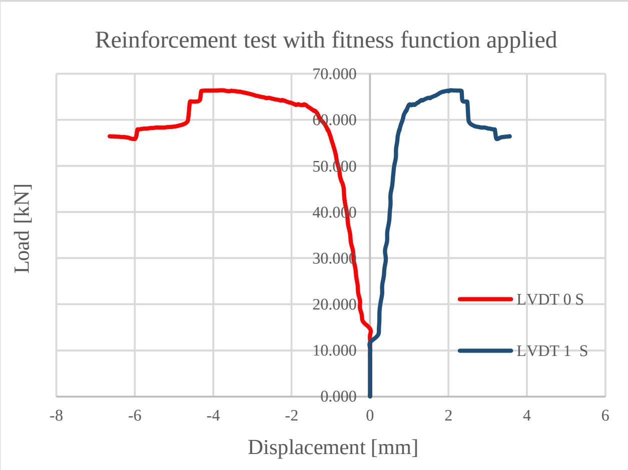

Fig. 22. Electronic scheme of LVDT WA-T [41]

The linearity variation in relation to nominal value of the DAQ is ±0.05 %, as a consequence it is negligible in the evaluation of the measurement accuracy with respect to the sensor linear characteristic. Instead, taking into consideration the linearity variation in relation to nominal value for the LVDTs is equal to ±0.500 mm [42-43]. This value must be reduced by dividing by √3 and identify a range of ±0.288 mm [44-45].

6. CONCLUSION

The principal aim of the paper is a preliminary research into the reliability and monitoring under dynamic loads of the technique patented by Pasquale Frezza. This type of anti-seismic construction consists in masonry walls built with bricks and fictile tubules, arranged in staggered and alternating manner, all contained in a timber wooden frame.

For the first specimen, tested until collapse, the experimental diagonal compression tests result in shear strengths is equal to 0.81 MPa and the lowering displacement recorded of the steel plate of the testing machine is equal to 11.526 mm. The second masonry wall was subjected to diagonal compression tests in two distinct phases. The specimen was first damaged, stopping the test when the first cracks appear, and then, it was repaired with B-FRCM and the test was repeated until collapse. The shear strengths obtained are respectively 0.73 MPa and 1.04 MPa. These results highlights as after the strengthening of the second specimen with B-FRCM, the shear strength registering an increase of 43% with respect to the unreinforced case, which point out the importance of fiber reinforcement for increasing the load-bearing capacity also in this kind of structures. However, both values are higher than the usual ones obtained for common masonry walls, and the cracks that formed are consistent with those expected from this type of test.

Figures 18 show the location of the cracks developed during the test of the first specimen at the attainment of the maximum load. On both sides of the masonry wall the cracks develop through mortar, parallel to each other and to the direction of application of the load, barely involving the fictile tubules. The numerical simulation shows good correspondence in terms of load-displacement diagram, with some minor discrepancies, and a development of cracks fairly mirroring the one obtained through the experimental test (Figure 18). In addition, the simulation of the damage in the wall obtained by means of a numerical model, corresponds discreetly to the experimental result. It shows (Figure 18) more cracks at the top and four single cracks departing from the middle section of each timber beam. Overall the model is very similar to the real one and the four cracks mentioned above appear, albeit small, in the back of the wall.

The displacement of the upper plate of the testing machine obtained with numerical model was compared with the experimental results to evaluate their compatibility. The linearity variation of the LVDT measurement with respect to their nominal values is equal to ±0.288 mm. In the experimental case, the measured displacement is equal to 11.526 ±0.866 mm, cover coefficient equal to 3. The displacement estimated by numerical model is compatible with the experimental tests (11.700 mm).

The Acquisition system proposed was composed by Linear Variable Differential Transformer (LVDT), used for monitoring the horizontal and vertical displacement, and strain gauges, used for monitoring the strain. These transducers were connected to data acquisition system (DAQ) Spider-8 which transmitted the data to a computer. All the data acquired are processed in real time with a spline fitness function in order to remove the disturbance caused by a noise due to the DAQ. In addiction a numerical model for these particular construction techniques was created in order to in order to start real-time analysis relating to the data recorded by the SHM system.

ACKNOWLEDGEMENT

The authors thank the engineers of "NGT Test "laboratory Gennaro Angotti, Cinzia Angotti e Dino Padula for the support in the tests.

REFERENCES

[1] F. Lamonaca, P. F. Sciammarella, C. Scuro, D. L. Carnì and R. S. Olivito, Internet of Things for Structural Health Monitoring, 2018 Workshop on Metrology for Industry 4.0 and IoT, Brescia, Italy, 2018, pp. 95-100.

[2] A. Barontini, M.G. Masciotta, L.F. Ramos, P. Amado-Mendes, P.B. Lourenço. An overview on nature-inspired optimization algorithms for Structural Health Monitoring of historical buildings. Procedia engineering, 199, (2017), pp. 3320-3325.

[3] C.R. Farrar, K. Worden, An introduction to structural health monitoring, Philosophical Transactions of the Royal Society of London A: Mathematical, Physical and Engineering Sciences, 365, (2007), pp. 303-315

[4] X.-H. Zhang, Y.-L. Xu, S. Zhu, S. Zhan, Dual-type sensor placement for multi-scale response reconstruction, Mechatronics, 24 (4) (2014), pp. 376-384

[5] C. Scuro, P.F. Sciammarella, F. Lamonaca, R.S. Olivito, D.L. Carnì, IoT for structural health monitoring. IEEE Instrumentation & Measurement Magazine, 21(6), (2018), pp. 4-14.

[6] X.-H. Zhang, Y.-L. Xu, S. Zhu, S. Zhan, Dual-type sensor placement for multi-scale response reconstruction, Mechatronics, 24 (4), (2014), pp. 376-384.

[7] A. Pierdicca, F. Clementi, D. Isidori, E. Concettoni, C. Cristalli, S. Lenci, Numerical model upgrading of a historical masonry palace monitored with a wireless sensor network, International Journal of Masonry Research and Innovation, 1(1), (2016), pp. 74-98.
[8] R. Kitchin, Big Data, new epistemologies and paradigm shifts. Big data & society, 1(1), (2014).
[9] E. Poletti, G. Vasconcelos, Seismic behaviour of traditional timber frame walls: experimental results on unreinforced walls. Bull Earthquake Eng, 13, (2015), pp.885–916.
[10] R. Langenbach R, From "Opus Craticium" to the "Chicago Frame": Earthquake-Resistant Traditional Construction. Int J Archit Herit, 1, (2007), pp.29–59
[11] E. Poletti, G. Vasconcelos, J.M. Branco, A.M. Koukouviki, Performance evaluation of traditional timber joints under cyclic loading and their influence on the seismic response of timber frame structures. Construction and Building Materials, 127, (2016), pp. 321-334.
[12] G. Vasconcelos, E. Poletti, E. Salavessa, A.M. Jesus, P.B: Lourenço, P. Pilaon, In-plane shear behaviour of traditional timber walls, Engineering Structures, 56, (2013), pp.1028-1048.
[13] E. Poletti, G. Vasconcelos, M. Jorge M, Application of near surface mounted (NSM) strengthening technique to traditional timber frame walls, Constr Build Mater, 76, (2015), pp. 34–50.
[14] S. Stellacci, V. Rato, E. Poletti, Structural Permanence in pre- and post-earthquake Lisbon: Half-timbered walls in overhanging dwellings and in pombalino buildings. Int J Archit Herit 11(3), (2017), pp.363–381.
[15] S. Tiberti, C. Scuro, S. Porzio, G. Milani, R.S. Olivito, Post-Cracking B-FRCM Strengthening of a Traditional Anti-Seismic Construction Technique (Casa baraccata): Extensive Experimental Investigations. In Key Engineering Materials, 817, (2019). pp. 634-641.
[16] C. Barucci, La casa antisismica: prototipi e brevetti. Gangemi Editore, Rome, 1990, ISBN10: 8874482914.
[17] G. Vivenzio, Istoria e teoria de' tremuoti in generale ed in particolare di quelli della Calabria, e di Messina del 1783. Stamperia Regale, 1783, Naples.
[18] C. Scuro, S. Tiberti, R. Codispoti, G. Milani, R.S. Olivito, Fictile tubules: A traditional Mediterranean construction technique for masonry vaulted systems. Construction and Building Materials, 193, (2018), pp. 84-96.
[19] R.S. Olivito, R. Codispoti, C. Scuro, A seismic analysis for masonry constructions: The different schematization methods of masonry walls. In AIP Conference Proceedings, Vol. 1906, No. 1, 2017, p. 090007. AIP Publishing LLC.
[20] S.Tiberti, C.Scuro, R.Codispoti, R.S.Olivito, G.Milani.. Experimental and numerical analysis of historical aseismic construction system. In Structural Analysis of Historical Constructions, 2019, pp. 910-918. Springer, Cham.
[21] C. Scuro, D.L. Carnì, F. Lamonaca, R.S. Olivito, G. Milani, An innovative structural health monitoring system for the preliminary study of an ancient anti-seismic construction technique. IMEKO TC-4 International Conference on Metrology for Archaeology and Cultural Heritage Florence, Italy, 2019, pp. 43-47.
[22] C. Calderini, S. Cattari, S. Lagomarsino, In-plane strength of unreinforced masonry piers, Earthquake Engineering and Structural Dynamics, 38(2), (2009), pp. 243-267.
[23] W. Mann, H. Müller, Failure of shear-stressed masonry – An enlarged theory, tests and application to shear-walls". Proc. of the International Symposium on Load bearing Brickwork, London, (1980), pp. 1-13.
[24] V. Turnšek, F. Čačovič, Some experimental results on the strength of brick masonry walls, Proc. of the 2nd International Brick Masonry Conference, Stoke-on-Trent, (1970), pp. 149-156.
[25] C. Calderini, S. Cattari, S. Lagomarsino, Identification of the shear mechanical parameters of masonry piers from diagonal compression test. In 11th Canadian Masonry Symposium, Toronto, Canada, 2009.
[26] C. Calderini, S. Cattari, S. Lagomarsino, The use of the diagonal compression test to identify the shear mechanical parameters of masonry. Construction and building materials, 24(5), (2010), pp. 677-685.
[27] S. Tiberti, C. Scuro, R. Codispoti, R.S. Olivito, G. Milani, Masonry structures built with fictile tubules: Experimental and numerical analyses. In AIP Conference Proceedings, Vol. 1906, No. 1, (2017). p. 090010). AIP Publishing LLC.
[28] P. Frezza, (1909), Construction System of Earthquake-Resistant Houses. Italian Patent 103254
[29] American Society for Testing and Materials (2015) ASTM E519 / E519M-15, Standard Test Method for Diagonal Tension (Shear) in Masonry Assemblages. doi: 10.1520/E0519_E0519M-15
[30] R.S. Olivito, R. Codispoti, C. Scuro, S. Porzio, Experimental evaluation of the adhesion of a FRCM-tuff strengthening system. Procedia Structural Integrity, 12, (2018), pp. 594-601.
[31] R.S. Olivito, R. Codispoti, C. Scuro, Experimental analysis on adhesion of NFRCM Systems applied to masonry structures, In AIMETA 2017 XXIII Conference the Italian Association of Theoretical and Applied Mechanics, Salerno, Italy, 2017, pp. 4-7.
[32] S. Tiberti, C. Scuro, R. Codispoti, R.S. Olivito, G. Milani, Post-cracking FRCM strengthening of an arch composed by hollow clay elements embedded in mortar: experimental investigations and numerical analyses. In Key Engineering Materials, Vol. 747, (2017), pp. 142-149.
[33] B. de Vries, J.M. Harink, Generation of a construction planning from a 3D CAD model. Automation in Construction, 16(1), (2007), pp.13-18.
[34] P.B. Lourenço, Recent Advances in Masonry Structures: Micromodelling and Homogenisation, in: U. Galvanetto, M.H.F. Aliabadi (Eds.), Multiscale Modeling in Solid Mechanics: Computational Approaches, Imperial College Press, London, United Kingdom, 2009, pp. 251-294.
[35] P. Lonetti, A. Pascuzzo, A. Davanzo, Dynamic behavior of tied-arch bridges under the action of moving loads. Mathematical Problems in Engineering, 2016, (2016), pp 17.
[36] S. Tiberti, M. Acito, G. Milani, Comprehensive FE numerical insight into Finale Emilia Castle behavior under 2012 Emilia Romagna seismic sequence: Damage causes and seismic vulnerability mitigation hypothesis, Engineering Structures, 117, (2016), pp. 397-421.
[37] A. Hillerborg, M. Modéer, P.E. Petersson, Analysis of Crack Formation and Crack Growth in Concrete by Means of Fracture Mechanics and Finite Elements, Cement and Concrete Research, 6 (6), (1976), pp. 773-781.
[38] J.G. Rots, J. Blaauwendraad, Crack Models for Concrete, Discrete or Smeared? Fixed, Multi-Directional or Rotating?, HERON 34 (1) (1989).
[39] P.Antunes, H.Lima, H.Varum, P.André. Optical fiber sensors for static and dynamic health monitoring of civil engineering infrastructures: Abode wall case study, Measurement: Journal of the International Measurement Confederation, 45 (7), (2012), pp. 1695-1705.
[40] HBM LVDT WA-T Data sheet
[41] HBM Spider-8 Data sheet.
[42] Guide to the Expression of Uncertainty in Measurement (GUM) (BIPM, IEC, IFCC, ILAC, ISO, IUPAC, IUPAP, and OIML) ISBN 92-67-10188-9, 1993.
[43] A. Katsuki, T. Sajima, H. Murakami, A.M. Hazrat, O. Ohnishi, K. Akashi, Development of a laser-guiding-type deep small-sized hole-measurement system: Measurement accuracy. Precision Engineering, 63, (2020), pp.18-32.
[44] S. Shi, B. Muralikrishnan, V. Lee, D. Sawyer, Methods to improve the dimensional measurement accuracy of a motion tracking system. Optics and Lasers in Engineering, 130, (2020),106092.
[45] C. Scuro, F. Lamonaca, R. Codispoti, D.L. Carnì, R.S. Olivito, Experimental and numerical analysis on masonry arch built with fictile tubules bricks. Measurement, 130, (2018), pp.246-254.